Study of Electrocatalysts for Oxygen Reduction Based on Electroconducting Polymer and Nickel

W. Martínez Millán, Mascha A. Smit

Materials Unit, Centro de Investigación Científica de Yucatán (CICY), Calle 43 No. 130, Col. Chuburná de Hidalgo, C.P. 97200, Mérida, Yucatán, México

Received 23 July 2008; accepted 6 December 2008
DOI 10.1002/app.29851
Published online 24 February 2009 in Wiley InterScience (www.interscience.wiley.com).

ABSTRACT: The properties and electrocatalytic activity were studied of composite carbon-supported materials based on heterocyclic polymer and nickel, in particular carbon/polyaniline/nickel, carbon/polypyrrole/nickel, carbon/poly(3-methylthiophene)/nickel, as well as their precursors, carbon/polyaniline, carbon/polypyrrole, and carbon/poly(3-methylthiophene). The materials were characterized by means of thermogravimetric analysis (TGA), scanning electron microscopy (SEM), EDAX, and electrochemical methods, such as cyclic voltammetry and linear voltammetry using RDE. SEM show porous materials, with a particle size of around 0.3 μm. It was found that in nickel-modified catalysts between 5 and 6 wt % of nickel is obtained. TGA and FTIR show that the modification with nickel alters the polymer bonds. Curves from cyclic voltammetry show cathodic peaks corresponding to the oxygen reduction reaction (ORR) in all materials, occurring at relatively low potentials. Based on the potential range for ORR as well as kinetic parameters obtained from linear voltammetry using RDE, it was concluded that C-Ppy-Ni shows the best performance for ORR in acidic medium.
 J Appl Polym Sci 112: 2959–2967, 2009

Key words: electroconductive polymer; electrocatalytic activity; electrocatalyst; oxygen reduction reaction; polyaniline; polypyrrole; poly(3-methylthiophene)

INTRODUCTION

The viability of new energy technology, and especially of hydrogen related technology, depends strongly on the development of new materials with improved properties. One group of such materials are electrocatalysts. Efficient, low cost, and stable electrocatalysts play an important role in fuel cells, for example, in the polymer electrolyte membrane fuel cell (PEMFC), with potential applications in transport and portable devices.[1]

The conventional PEM catalyst is a carbon-supported platinum-based material, and may include other precious metals.[2,3] This material shows high electrocatalytic activity for many electrochemical reactions, but also has high cost and in some conditions may have problems in stability. Therefore, on-going research exists into low-cost and abundant alternative catalyst materials. Several precious metal-free materials have been suggested for the cathode of a PEMFC,[4–8] but very few materials have electrocatalytic activity for the oxygen reduction reaction (ORR)[9] and even less with sufficient long term stability.

It has been observed that pyrolized cobalt porphyrins show good electrocatalytic activity for ORR.[4,7–9] Studies on these materials suggest that these cobalt porphyrins have species of the type $Co{-}N_X$, being the active sites for the ORR.[6,10–12]

At the same time, recent attention has been drawn to catalysts based on electroconducting polymers, due to their range of properties and low cost when compared with precious metals. Conjugated heterocyclic polymers such as polyaniline (Pani), polypyrrole (Ppy), and poly(3-methylthiophene) (P3MT) have been the subject of many investigations, due to their potential use in areas such as electronics,[13] biosensors and actuators,[14] electrochemistry and electrocatalysis,[15] etc. These materials show characteristic and reversible changes of conductivity and other properties under oxidation and reduction (switching). Most of these polymers have shown some electrocatalytic activity for the ORR in acidic media (pH < 7).[11] Recently, new catalytic materials for ORR have been reported based on conducting polymers,[16] conducting polymers doped with heteropolyanions and metallic complexes,[17–19] and conducting polymers modified with catalysts of noble metals.[18,20]

The insertion of metal atoms, such as cobalt or nickel, into the structure of the electroconductive polymers PAni and Ppy would mimic the atomic

Correspondence to: M. A. Smit (mascha@cicy.mx).
Contract grant sponsor: Conacyt; contract grant numbers: 47066-Y, QROO-18975.

configuration of cobalt-containing porphyrins, with the metal atom being linked to the monomer units, thus allowing for the formation of Co—N or Ni—N sites for ORR, without destroying the structure of the initial polymer.[6] In the case of poly(3-methylthiophene), it is assumed that active Co—S or Ni—S sites are generated. In previous studies of electroconductive polymer-cobalt composites based on polypyrrole (Ppy), polyaniline (Pani), and poly(3-methylthiophene) (P3MT) modified with cobalt, it was found that the material with best performance for ORR in acidic medium was carbon/polypyrrole/cobalt.[21]

In this document, the synthesis and study of catalytic nanocomposites of heteroatomic polymer and nickel supported on carbon black is presented for potential application as cathode materials in PEMFCs. The polymers studied are nickel-modified polyaniline, polypyrrole, and poly(3-methylthiophene), synthesized via chemical method. Results for the corresponding nickel-free materials are shown for the reasons of comparison. The presumed configuration of the composites with nickel are assumed to be similar to structures reported previously,[6,21] with nickel replacing the cobalt atoms.

EXPERIMENTAL

Synthesis

The synthesis of the composite carbon-supported materials was carried out as follows[6,21]: 8 g of carbon black (Vulcan XC-72) was mixed with 60 mL of distilled water and 2 mL of glacial acetic acid and stirred for 20 min at room temperature. 2 g of the monomer was added and stirred for 5 min. The monomer was either aniline, pyrrole, or 3-methylthiophene (all obtained from Sigma-Aldrich, 99%). This was followed by the addition of 14 mL of H_2O_2 (30%) as an oxidant. The mixture was stirred during 3 h at room temperature. The carbon black-polymer composite was filtered, washed with warm distilled water, and dried at 100°C in air during 24 h. Finally, 4.5 g of the composite was mixed with 100 mL of distilled water in a three-necked round-bottomed flask, stirring for 10 min. The resulting dispersion was heated under reflux to 80°C, and then 25 mL of 0.3*M* of a $Ni(NO_3)_2{\cdot}6H_2O$ solution was added. The obtained mixture was stirred vigorously for 30 min at 80°C, followed by the addition of 500 mL of reducing agent (5.23 g of $NaBH_4$ and 0.37 g of NaOH in 500 mL of distilled water) (pH 11.4), added at a rate of 20 mL per minute. The catalyst was filtered and washed repeatedly with distilled water at 50°C until the pH of the filtrate reached 7.0, and finally, it was dried in air at 100°C during 24 h.

Cathode catalyst ink was prepared mixing the carbon-polymer-nickel composite with distilled water to achieve a 1 : 10 ratio by weight and adding recast Nafion® ionomer (5% Nafion® 1100 suspension in alcohol, Fluka Corp.) to reach a 1 : 1 volumetric ratio. The mixture was placed in an ice bath to prevent overheating and minimize evaporation of solvents, and ultrasonically mixed for 5 min. Next, by means of a graduated micropipette, 2 μL of the cathode ink was deposited on a rotational disk electrode with an active area of 0.071 cm^2 (representing 0.6 mg/cm^2).

Based on this procedure, the following composite materials were synthesized: carbon/polyaniline (C-Pani); carbon/polyaniline/nickel (C-Pani-Ni); carbon/polypyrrole (C-Ppy); carbon/polypyrrole/nickel (C-Ppy-Ni); carbon/poly(3-methylthiophene) (C-P3MT); and carbon/poly(3-methylthiophene)/nickel (C-P3MT-Ni).

Characterization

Thermogravimetric analysis (TGA) was carried out in nitrogen atmosphere on a Perkin–Elmer equipment model TGA7 at 10°C min^{-1}.

The morphological and compositional characterization was performed by using scanning electron microscopy (SEM) on a JEOL Microscope Model JSM-6360 LV at 20 KV and equipped with an INCA Energy 200 microprobe.

Fourier-transform infrared (FTIR) spectra were obtained using a FTIR Perkin–Elmer spectrophotometer, Spectrum GX. The tests were made in the 2000–650 cm^{-1} interval, with a resolution of 4 cm^{-1}, a scan rate of 0.63 cm^{-1} s^{-1}, and 15 sweeps per sample.

The electrochemical characterization was carried out in a standard three-electrode electrochemical cell with either a stationary or a rotating disk working electrode (characteristics and preparation commented previously). As counter electrode, a graphite electrode was used, and a standard saturated calomel electrode (SCE) was used as a reference electrode (+0.241 V versus NHE). The potentiostat used was an Autolab Pgstat302N.

Cyclic voltammetry was carried out using a stationary electrode in 0.5*M* H_2SO_4 at room temperature, saturated with either nitrogen or oxygen, in a potential range between −209 mV and 1041 $mV_{H/H+}$ and with a scan rate of 20 mV/s.

Cathodic potentiodynamic curves were obtained at a scan rate of 1 mV/s, using a RDE at 0, 200, 400, 600, 800, and 1800 rpm. Tests were performed in 0.5*M* H_2SO_4 at room temperature, saturated with either nitrogen or oxygen. Curves were started from the open circuit potential, E_{oc}, down to the potential at which the current density reached its maximum on the ORR peak, as determined from cyclic voltammetry for each sample.

Potentiostatic tests were carried out applying the maximum potential obtained from cyclic

voltammetry in the ORR peak, using a stationary electrode, to determine stability. All potentials are reported versus NHE.

RESULTS AND DISCUSSION

Thermogravic analysis

Figure 1 shows the results obtained from TGA. Carbon black was included as a reference material and shows a stable region at low temperature followed by rapid decomposition at ~ 650°C. The curves obtained for the nickel-free carbon/polymer samples (C-Pani, C-Ppy, C-P3MT) have similar shape as the curve for carbon black, though with increased mass loss in the low temperature region related to polymer degradation, and faster decomposition in the high temperature region related to carbon degradation. The curves for C-Pani and C-Ppy are very similar in shape, and show rapid decomposition starting at around 570°C, whereas C-P3MT starts rapid decomposition at 650°C, the same temperature as for carbon black.

The nickel-containing samples C-Pani-Ni, C-Ppy-Ni, and C-P3MT-Ni show a faster initial mass loss, when compared with the nickel-free samples. However, the three nickel-containing samples do not show the rapid decomposition at high temperature related to the carbon decomposition. This indicates that at lower temperatures, the decomposition of these materials appears to be activated in the presence of nickel and may be related to the degradation of nickel compounds, such as nickel oxides.[22] At higher temperatures, however, thermal stability is improved when compared with carbon black and nickel-free samples.

FTIR

Figure 2 shows FTIR spectra obtained for carbon/polymer and carbon/polymer/cobalt samples. For all samples, most of the bands in the spectra correspond to carbon black. For example, bands in the ranges of: 1534–1548 cm^{-1}, 1457–1464 cm^{-1}, 1397–1399 cm^{-1}, 1220–1226 cm^{-1}, and 835–848 cm^{-1} are related to the C—C vibrations.[23,24]

In the case of C-Pani [Fig. 2(a)], apart from carbon related bands, there are some bands which correspond to polyaniline, for example, bands in the range of 1950–1800 cm^{-1}, 1187, and 1158 cm^{-1} are related to different C—H vibrations,[23] a band at 1399 cm^{-1} corresponds to the stretching of C—N between rings, and a band at 1548 cm^{-1} is related to C—C vibrations inside the benzenoid ring.[24,25] The strong band seen at 1651 cm^{-1} could be related to C=O stretching in carboxyl or amide groups, and at 1112 cm^{-1} may be related to C—N and C—O stretching vibration,[26] however, a number of bands overlap with peaks of the carbon black matrix.

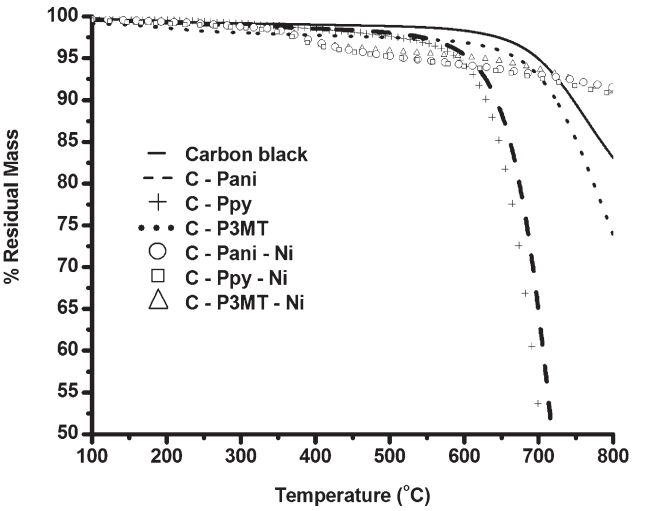

Figure 1 TGA curves obtained in nitrogen atmosphere.

FTIR bands corresponding to the C-Ppy sample [Fig. 2(b)] are less intense than for C-Pani. Bands at 747 cm^{-1} are related to C—H vibrations.[27,28] There is a band near 1220 cm^{-1} related to C—N vibration, which appears to overlap with the carbon black matrix vibrations. A strong peak seen at 1682 cm^{-1} corresponds to C=O bonds and C—N and C—O stretching vibrations can be found at 1132 cm^{-1}.

In the case of C-P3MT, [Fig. 2(c)], bands are as pronounced as for C-Pani. Bands at 797 and 675 cm^{-1} are related to the thiophene ring,[29,30] and the band at 727 cm^{-1} is attributed to C—H vibrations. Bands near 1550 and 1457 cm^{-1} are related to 3-methylthiophene ring vibration.[28] Again, overlap exists with bands corresponding to the carbon black. A strong band at 1660 cm^{-1} is related to the C=O group and at 1097 cm^{-1} to the C—O bond.[27]

For the nickel-containing samples, C-Pani-Ni, C-Ppy-Ni, and C-P3MT-Ni [Fig. 2(d–f)], it can be seen that most bands occur at the same wavenumbers as for their nickel-free precursors, but with a difference in intensity for a number of bands.[28] All nickel-containing samples show an increased amount of peaks at lower wavenumbers, such as 854–857 cm^{-1}, which may be related to Ni—N or Ni—S bonds. Bands located around 1650–1680 cm^{-1}, 1230 cm^{-1}, and 1100–1130 cm^{-1}, related to C—O and C—N bonds respectively, appear with increased intensity and have shifted to lower wavenumbers for nickel-containing samples, which has been related to the preferential formation of nickel-nitrogen or nickel-oxygen bonds.[26]

According to the proposed structures,[6,21] nitrogen and sulfur atoms are the main sites for nickel attachment, because it is assumed that nickel does not easily attach to carbon, as reported previously.[27] Alternatively, oxygen atoms in the carboxylic or hydroxyl groups may form nickel bonds. In either

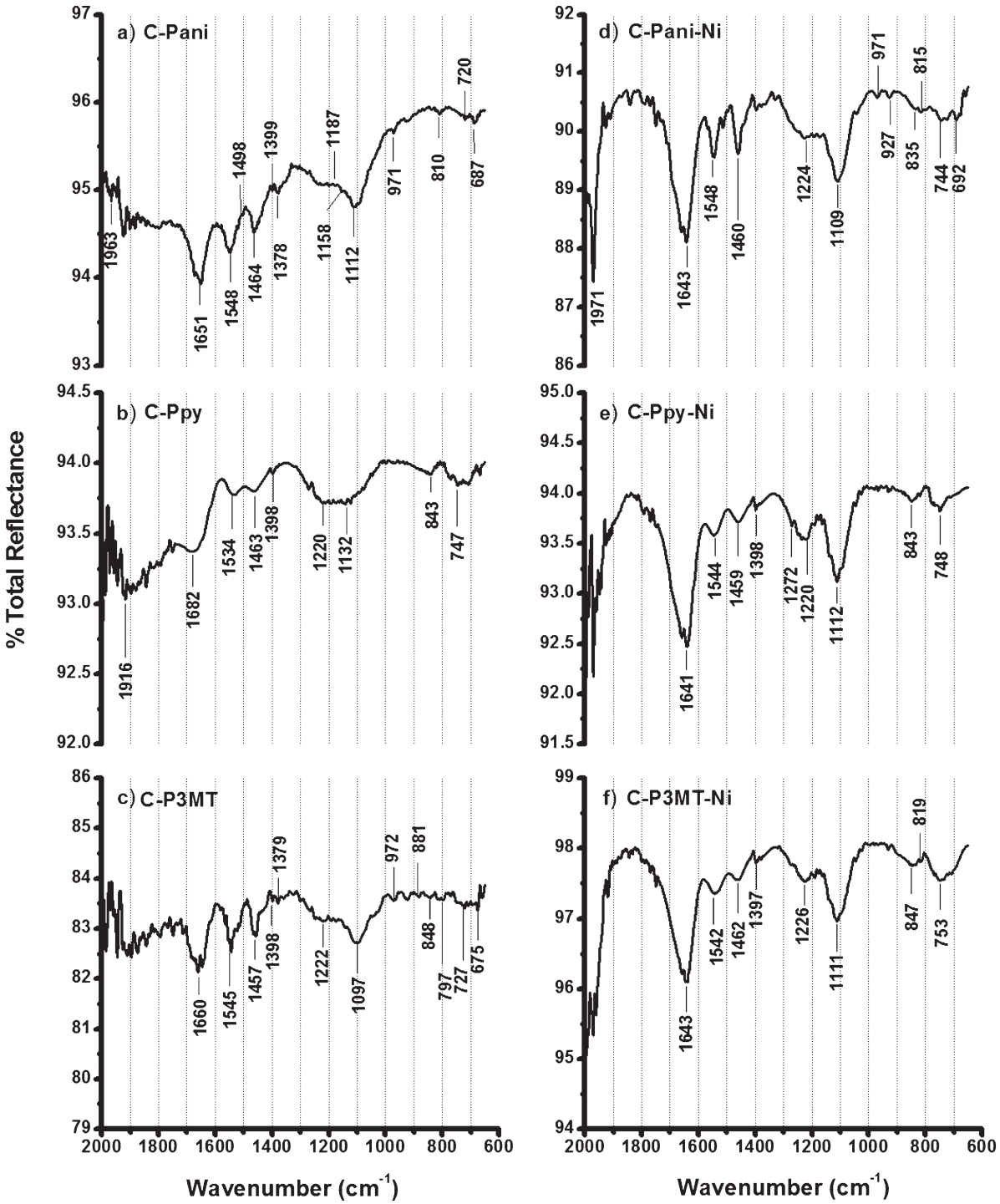

Figure 2 FTIR spectra obtained for: (a) C-Pani; (b) C-Ppy; (c) C-P3MT; (d) C-Pani-Ni; (e) C-Ppy-Ni, and (f) C-P3MT-Ni.

case, the functional groups of NH, and probably CO, present at the sample surface, are involved in nickel bonding.

Morphology and elemental analysis

Figure 3 shows SEM micrographs for carbon black [Fig. 3(a)], C-Ppy [Fig. 3(b)], and C-Ppy-Ni [Fig. 3(c)]. It is observed that for all samples very similar morphology is obtained. Small spherical grains are observed for all the materials, without any significant difference in morphology or particle size. The spherical grains have diameters between 0.50 and 0.12 μm. Lighter areas are related to charging of the samples, and EDAX confirmed that the composition in these areas is the same as in darker areas.

Table I shows the chemical composition in weight percent obtained by EDAX for the elements found in

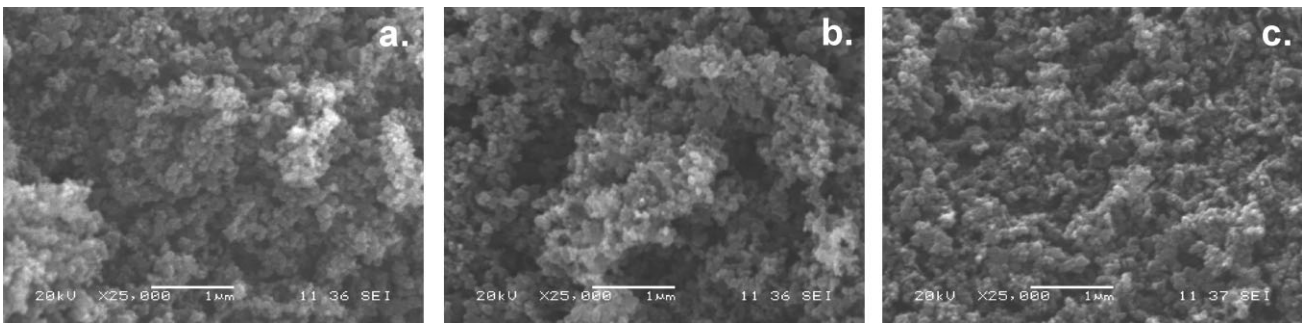

Figure 3 SEM images of: (a) carbon black; (b) C-P3MT; and (c) C-P3MT-Ni.

the samples. All data is averaged and rounded for the entire area shown in the images in Figure 3. According to the table, carbon is present in quantities which vary from 88 to 92%, very close to the calculated values based on initial reactant ratios. There are significant quantities of oxygen in all samples. The oxygen is assumed to be present on the carbon surface as oxygen functional groups, such as the carbonyl, carboxylic, phenolic, anhydride, lactonic, and etheric groups.[22] The C-P3MT and C-P3MT-Ni samples have sulfur in small quantities (1% in weight), which is less than expected, based on the initial ratios (5% for C-P3MT and 4% for C-P3MT-Ni), indicating that only a small amount of polymer is present. The nickel content in nickel-containing samples is of the same order as the cobalt content found in cobalt-containing polymers.[21] For C-P3MT-Ni, it can be observed that the Ni : S ratio (5 : 1 in weight) does not correspond to the proposed structure, which would have an atomic ratio of 1 : 1, equivalent to a ratio of around 2 : 1 in weight. Therefore, the amount of nickel in this sample is almost three times higher than the proposed structure allows, indicating that other nickel compounds are present, possibly nickel oxides and/or hydroxides. This is confirmed by TGA and FTIR results, because in TGA fast, initial mass loss was related to the presence of nickel compounds, such as nickel oxides[22] and in FTIR, increased and shifted CO bonds were related to the presence of nickel-oxygen bonds.[26]

Electrochemical characterization

In Figure 4, the results of cyclic voltammetry for the heterocyclic polymer-nickel samples are shown. The arrows show the scanning direction, the scan rate was 20 mV/s. The continuous lines correspond to oxygen saturated environment and the dashed lines to oxygen-free atmosphere (under nitrogen). In oxygen-free electrolyte, curves show characteristic polymer oxidation and reduction,[15,16] as well as some hydrogen evolution at low potentials. Under oxygen, ORR peaks can be seen in the cathodic zone for all the materials. The curve for carbon black is not shown, because it does not show ORR electrocatalytic activity.[22]

Polyaniline shows small current densities for both the unmodified and nickel-modified samples, as observed also for cobalt modified polyaniline.[21] Two distinct oxidation and reduction peaks can be seen as related to the transitions from leucoemeraldine to emeradine and, subsequently, from emeraldine to pernigraniline, and vice versa. The second reduction peak occurs at low potentials, below 300 mV, just before the oxygen reduction in oxygen containing environment starts. This coincides with reports that electrocatalitic activity for reduction reactions is seen when polymers are in the reduced state.[16] In the case of polypyrrole and poly(3-methylthiophene), the curves are very similar in shape. The higher current densities indicate higher electroactivity when compared with polyaniline. For these materials, as expected, only one peak for polymer oxidation is seen, at around 500 mV. In the case of polypyrrole, the reduction peaks cannot be observed, whereas for poly(3-methylthiophene) these occur around 450 mV, before the onset of oxygen reduction.

To determine which material has the highest ORR electrocatalytic activity (by electrode area), the difference between the maximum current density on each ORR peak and the current density in its base are calculated. The highest difference is observed for C-Ppy-Ni, indicating highest electrocatalytic activity, with a difference in current densities of 2.4 mA/

TABLE I
Chemical Composition in Weight Percent as Obtained by EDAX

	Weight (%)				
Sample	C	O	S	Ni	Total
Carbon black	94	6	–	–	100
C-Pani	92	8	–	–	100
C-Ppy	90	10	–	–	100
C-P3MT	89	10	1	–	100
C-Pani-Ni	89	6	–	5	100
C-Ppy-Ni	89	6	–	5	100
C-P3MT-Ni	88	6	1	5	100

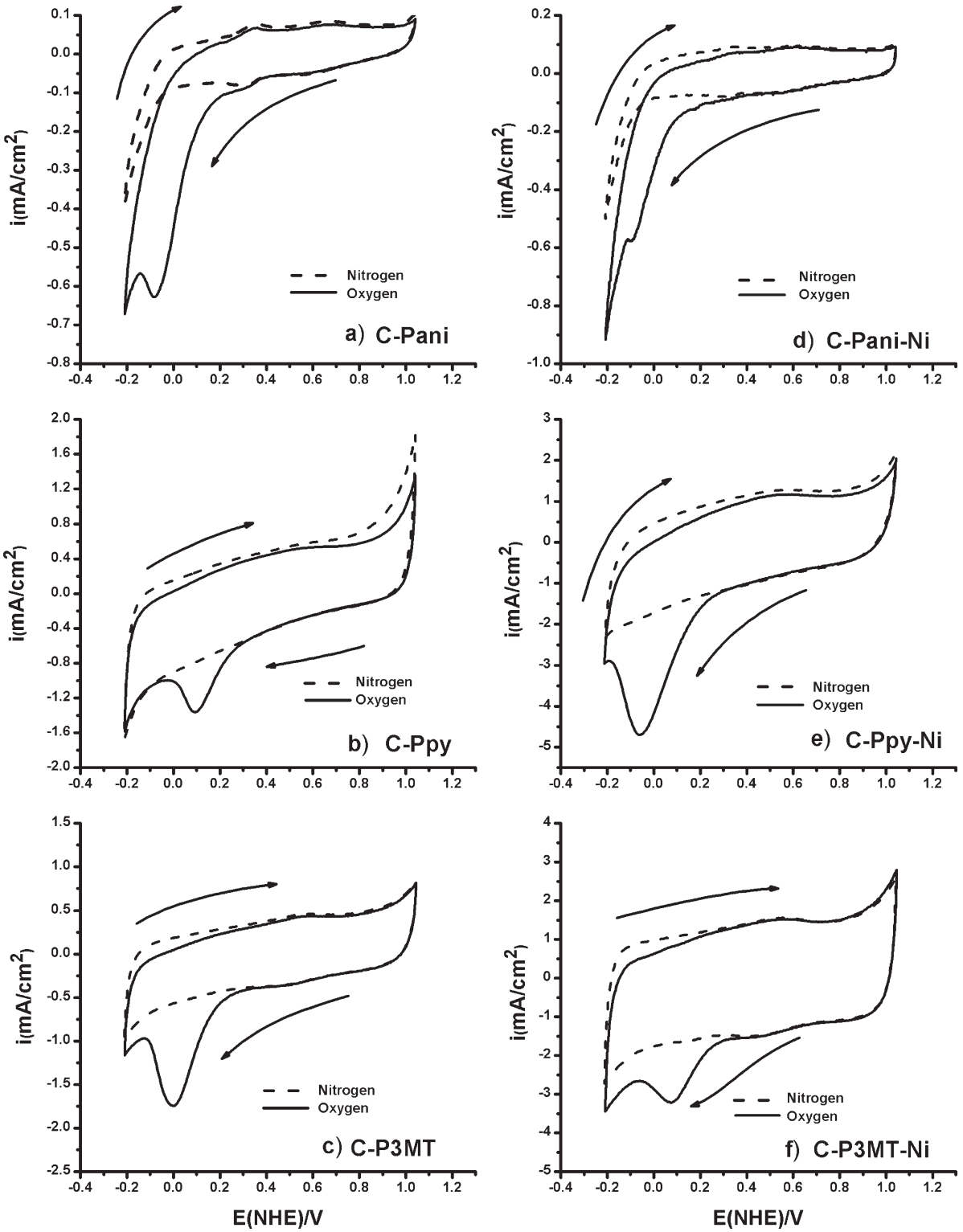

Figure 4 Cyclic voltammetry for: (a) C-Pani; (b) C-Ppy; (c) C-P3MT; (d) C-Pani-Ni; (e) C-Ppy-Ni, and (f) C-P3MT-Ni. Tests carried out at room temperature in 0.5*M* H_2SO_4 at 20 mV/s.

cm^2, followed by C-P3MT-Ni with a difference of 1.0 mA/cm^2 and C-P3MT with 0.99 mA/cm^2. Lower activity is found for C-Ppy with 0.56 mA/cm^2, C-Pani and C-Pani-Ni samples with 0.19 mA/cm^2 and 0.048 mA/cm^2, respectively.

Figure 5 shows the oxygen reduction current densities for C-Polymer-Ni electrodes, obtained from linear voltammetry with a rotating disk electrode system, in 0.5 M H_2SO_4 at a scan rate of 1 mV/s. The experiments were carried out starting from the

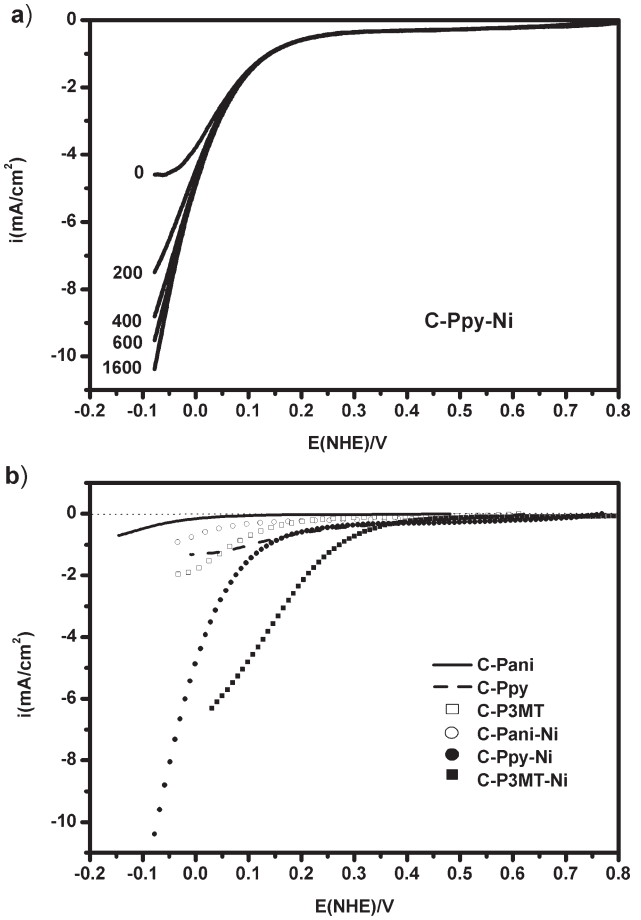

Figure 5 Results from rotating disk voltammetry for polymer-nickel samples, carried out at 1 mV/s in 0.5*M* H_2SO_4 saturated with oxygen: (a) for C-Ppy-Ni at 0, 200, 600, 800, and 1600 rpm; (b) for different samples at 1600 rpm.

open circuit potential (E_{oc}) down to the potential where highest current density on the ORR peak was obtained in cyclic voltammetry (see Fig. 4). In Figure 5(a), results are shown for C-Ppy-Ni at rotation speeds of 0, 200, 600, 800, and 1600 rpm. As expected, at lower potentials, increasing rotation speed leads to increasing current density. This behavior was observed for all samples. In Figure 5(b), a comparison of results obtained for different samples at 1600 rpm under oxygen atmosphere is presented.

In the polarization curves in semistationary state as shown in Figure 5(a) for C-Ppy-Ni, three areas can be identified. At lower overpotentials between 0.8 and 0.05 V, the electron transfer is slow when compared with mass transport. A second area is seen at high overpotentials beyond −0.062 V, showing diffusion limited current densities depending on the rotation speed. A region of mixed control is observed between 0.05 and −0.062 V. With i_K the current density controlled by the charge transfer and i_L the current density controlled by mass transfer, the total current density can be expressed by a first order kinetic relationship[2,3]:

$$\frac{1}{i} = \frac{1}{i_K} + \frac{1}{i_L} \tag{1}$$

which, based on the Levich equation, can be expressed as:

$$\frac{1}{i} = \frac{1}{nFkAC_{O_2}} + \frac{1}{0.62nFD_{O_2}^{2/3}AC_{O_2}V^{1/6}\omega^{1/2}} \tag{2}$$

where n is the electron number involved in the ORR, Co_2 is the oxygen concentration, Do_2 is the oxygen diffusion coefficient in the medium, ω the electrode rotation speed, and k is the global rate constant of the reaction.

Using eq. (1) to obtain the average kinetic current density, i_k, the following kinetic parameters were determined: Tafel slope (b), transfer coefficient (α_c), and exchange current density (i_o).[2,3,31] Results are shown in Table II and include the open circuit potential, E_{oc}.

C-P3MT-Ni and C-Ppy-Ni electrodes have the highest open circuit potentials (E_{oc}), with 0.85 and 0.8 V, respectively, followed by C-Pani-Ni with 0.76 V and at last C-P3MT, C-Ppy, and C-Pani with 0.63, 0.62, and 0.48 V, respectively.

The Tafel slopes and load transfer coefficients are very similar among the different samples. However, C-Ppy-Ni has the highest exchange current density with 4×10^{-5} mA/cm^2, followed very close by C-P3MT-Ni with 3.5×10^{-5}, and C-Ppy with 2.46×10^{-5} mA/cm^2.

All Tafel slopes have values between 0.111 and 0.120 V/dec. Tafel slopes inside the range from −0.120 to −0.150 V/dec (at room temperature) indicate that the first electron transfer is the decisive step in the global ORR.[2]

To further compare the performance of these materials as oxygen reduction catalyst, the potentials at which oxygen reduction takes place were compared. Therefore, the potentials at which maximum current density occurred in cyclic voltammetry (Fig. 4) were determined and are also listed in Table II.

TABLE II
Electro Kinetic Parameters Obtained from RDE Experiments

Electrode	E_{oc} (V/NHE)	$-b$ (V/dec)	α	i_o (mA/cm^2)	E (mV) at i_{max} ORR
C-Pani	0.48	0.115	0.49	2.34×10^{-6}	−87
C-Ppy	0.62	0.111	0.48	2.46×10^{-5}	93
C-P3MT	0.63	0.120	0.49	1.00×10^{-5}	1
C-Pani-Ni	0.76	0.116	0.50	1.00×10^{-6}	−92
C-Ppy-Ni	0.80	0.117	0.56	4.00×10^{-5}	−62
C-P3MT-Ni	0.85	0.117	0.55	3.50×10^{-5}	74

It can be seen that highest potential is obtained in the order of C-Ppy > C-P3MT-Ni > C-P3MT. For PAni and Ppy, the addition of nickel shifts the ORR reaction to more negative potentials, while only for P3MT the potential shifted to higher values, as found for similar cobalt-containing samples.[21] This may be related to the creation of active Ni—S sites. Even so, the active potential range is well below the required range for application in fuel cells.

Based on these data, C-Ppy, C-Ppy-Ni, and C-P3MT-Ni show best performance for the ORR, with C-Ppy-Ni showing highest exchange current density and C-Ppy having the most positive potential range for ORR. C-P3MT-Ni shows both a high exchange current density and relatively high potential range for ORR.

Results for similar composite materials prepared with cobalt, instead of nickel, have been reported elsewhere.[21] For the polyaniline containing samples, the addition of nickel leads to similar results as for cobalt in terms of exchange current density and potential for maximum ORR; however, slightly better results for both parameters are obtained with cobalt. In both cases (nickel and cobalt), the lowest exchange current densities are found for Pani composites. For nickel-modified polypyrrole, the potential for maximum ORR is much lower as for cobalt-containing samples (−62 and 325 mV, respectively), and even lower as for unmodified C-Ppy (93 mV). The exchange current density, however, is highest for C-Ppy-Ni. In the case of poly(3-methylthiophene), the exchange current densities are of the same order for nickel- and cobalt-modified samples, whereas the maximum current potential is highest for the nickel-containing sample. Therefore, it can be concluded that in the case of poly(3-methylthiophene), the modification with nickel improves performance for the ORR when compared with unmodified and cobalt-modified poly(3-methylthiophene).

To determine the stability of the nickel-containing materials in the acid environment during oxygen reduction, chronoamperometry was carried out during 2 days (see Fig. 6), applying for each sample the potential at which the maximum current density for ORR was observed from cyclic voltammetry (see Fig. 4 and Table II). For C-Ppy, a continuous decrease is observed, indicating a possible slow degradation of the sample. However, for C-Ppy-Ni and C-P3MT-Ni, after an initial decrease in current response during the initial hours, a very stable density current is observed in both electrodes, indicating good stability in the acid, oxygen rich environment.

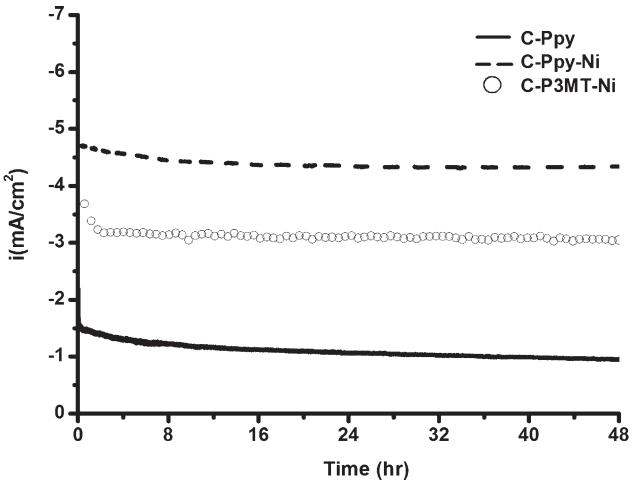

Figure 6 Chronoamperometric curves for C-Ppy, C-Ppy-Ni, and C-P3MT-Ni in 0.5*M* H_2SO_4 under oxygen.

CONCLUSIONS

The electrocatalytic activity for the oxygen reduction reaction in acid medium was studied for carbon-supported materials based on different heterocyclic polymers modified with nickel.

SEM images showed no significant change for the carbon/polymer and carbon/polymer/nickel samples, when compared with the carbon black morphology. Changes in the FTIR bands suggest the existence of Ni—N bonds (for polyaniline and polypyrrole-based samples) and Ni—S bonds (for poly (3-methylthiophene)-based samples). TGA results reveal that the addition of nickel reduces the thermal stability in an intermediate temperature range, possibly related to the presence of nickel oxides or hydroxides, or carboxylic groups, but improves stability at high temperature, suggesting modification of the carbon support.

Based on cyclic voltammetry, it was determined that all materials have electrocatalytic activity for the ORR. The addition of nickel results in more positive potentials for ORR for C-P3MT, and in the case of C-Ppy-Ni and C-P3MT in improved electrocatalytic activity. The potential at which ORR occurs was determined to be highest for C-Ppy, followed by C-P3MT-Ni. Lowest potential range for ORR was found for the polyaniline containing materials.

Kinetic parameters, calculated from lineal voltammetry tests using RDE, show that C-Ppy-Ni, C-P3MT-Ni, and C-Ppy have highest exchange current densities. All samples have Tafel slopes between −110 and −120 V/dec, which indicate that the first electron transfer is the decisive step in the global ORR. Based on exchange current densities, it is concluded that C-Ppy-Ni presents the best electrocatalytic sites for ORR, whereas C-Ppy shows the most positive potential range for ORR. C-P3MT-Ni shows both relatively high exchange current density and potential range for ORR. However, the potential range for ORR still needs to be shifted further upwards, before being able to apply these materials

in commercial fuel cell systems. Chronoamperometry shows an adequate electrochemical stability of the nickel-modified samples to be used as cathode catalyst in acid medium for ORR.

We are grateful to Tanit Toledano T. and Wilberth Herrera K. for their help in SEM, TGA, and FTIR. And also, we would like to thank the CIE-UNAM for the facilities provided for the realization of part of this work.

References

1. Jacobson, M. Z.; Collela, W. G.; Gonden, D. M. Science 2005, 308, 1901.
2. González-Huerta, R. G.; Leyva, M. A.; Solorza-Feria, O. Rev Soc Quím Méx 2004, 48, 1.
3. Cao, D.; Wieckowski, A.; Inukai, J.; Alonso-Vante, N. J Electrochem Soc 2006, 153, A869.
4. Wang, B. J Power Sources 2005, 152, 1.
5. Atanososky, R. Report VIIC9, US DOE, 2005.
6. Bashyam, R.; Zelenay, P. Nat Lett 2006, 443, 63.
7. Lee, K.; Zhangi, J.; Wang, H.; Wilkinson, D. P. J Appl Electrochem 2006, 36, 507.
8. Villers, D.; Jacques-Bedard, X.; Dodelet, J. P. J Eletrochem Soc 2004, 151, A1507.
9. Medard, C.; Lefevre, M.; Dodelet, J. P.; Jaouen, F.; Lindbergh, G. Electrochim Acta 2006, 51, 3202.
10. Faubert, G.; Lalande, G.; Cote, R.; Guat, D.; Dodelet, J. P.; Weng, L. T.; Bertrand, P.; Denes, G. Electrochim Acta 1996, 41, 1689.
11. Yamamoto, K.; Taneichi, D. J Inorg Organomet Polym 1999, 9, 231.
12. Beck, F. J Appl Electrochem 1977, 7, 239.
13. Gurunathan, K.; Murugan, A. V.; Marimuthu, R.; Mulik, U. P.; Amalnerkar, D. P. Mater Chem Phys 1999, 61, 173.
14. Schultze, J. W.; Karabulut, H. Electrochim Acta 2005, 50, 1739.
15. Careema, M. A.; Velmurugu, Y.; Skaarup, S.; West, K. J Power Sources 2006, 159, 210.
16. Khomenko, V. G.; Barsukov, V. Z.; Katashinskii, A. S. Electrochim Acta 2005, 50, 1675.
17. Cong, H. N.; El Abbassi, K.; Gautier, J. L.; Chartier, P. Electrochim Acta 2005, 50, 1369.
18. Alonso-Vante, N.; Cattarin, S.; Musiani, M. J Electroanal Chem 2000, 481, 200.
19. Singh, R. N.; Lal, B.; Malviya, M. Electrochim Acta 2004, 49, 4605.
20. Lai, E. K.; Beattie, P. D.; Holdcroft, S. Synth Met 1997, 84, 87.
21. Martínez, W.; Toledano-Thompson, T.; Arriaga, L.G.; Smit, M. A. Int J Hydrogen Energy 2009, 34, 694.
22. Bezerra, C. W.; Zhang, L.; Liu, H.; Lee, K.; Marques, A. L. B.; Marques, E. P.; Wang, H.; Zhang, J. J Power Sources 2007, 173, 891.
23. Trchova, M.; Sedeonkova, I.; Stejskal, J. Synth Met 2005, 154, 1.
24. De, S.; Dey, A.; De, S. K. J Phys Chem Solids 2007, 68, 66.
25. Romero-García, J.; Cruz-Silva, R.; Ruiz-Flores, C.; Arias-Marín, E.; Ledezma-Pérez, A.; Moggio, I.; Flores-Loyola, E. Rev Mex de Ing Quím 2003, 2, 173.
26. Panda, G. C.; Das, S. K.; Bandopadhyay, T. S.; Guha, A. K. Colloids Surf 2007, 57, 135.
27. Ando, E.; Onodera, S.; Iino, M.; Ito, O. Carbon 2001, 39, 101.
28. Smith, L. A. Applied Infrared Spectroscopy, Fundamentals, Techniques, and Analytical Problem solving; Wiley: New York, 1974.
29. Park, D. H.; Kim, B. H.; Jang, M. G.; Bae, K. Y.; Joo, J. Appl Phys Lett 2005, 86, 113.
30. Nicho, M. E.; Hu, H.; Lopez-Mata, C.; Escalante, J. Sol Energy Mater Sol Cells 2004, 82, 105.
31. Alonso-Vante, N.; Tributsch, H.; Solorza-Feria, O. Electrochim Acta 1995, 40, 567.